Journal of Materials Chemistry A

Accepted Manuscript

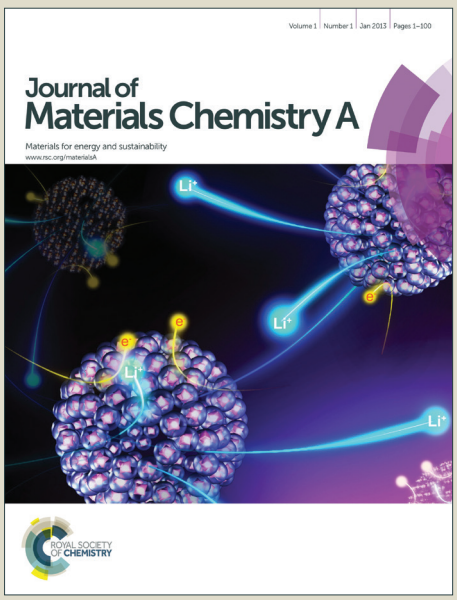

ROYAL SOCIETY OF CHEMISTRY

www.rsc.org/materialsA

Journal Name

RSCPublishing

ARTICLE

A novel composite polymer electrolytes containing poly(ethylene glycol)-grafted graphene oxide for all-solid-state lithium-ion battery applications

Cite this: DOI: 10.1039/x0xx00000x

Received 00th January 2012,
Accepted 00th January 2012

DOI: 10.1039/x0xx00000x

www.rsc.org/

Jimin Shim, Dong-Gyun Kim, Hee Joong Kim, Jin Hong Lee, Ji-Hoon Baik and Jong-Chan Lee*

A series of composite polymer electrolytes were prepared using organic/inorganic hybrid branched-graft copolymer (BCP) based on poly(ethylene glycol) methyl ether methacrylate (PEGMA) and 3-(3,5,7,9,11,13,15-heptaisobutylpentacyclo-[9.5.1.13,9.15,15.17,13]octasiloxane-1-yl)propyl methacrylate (MA-POSS) as polymer matrix and poly(ethylene glycol)-grafted graphene oxide (PGO) as filler materials, and they were applied to solid-state polymer electrolyte (SPE) for lithium-ion battery applications. The ionic conductivity of the composite polymer electrolyte containing 0.2 wt% of PGO (2.1×10^{-4} S/cm at 30 °C) was found to be one order of magnitude higher than that of the BCP (1.1×10^{-5} S/cm at 30 °C), the pristine polymer matrix, because larger amount of lithium salt can be dissociated in the composite polymer electrolyte by Lewis acid-base interaction between the PGO and lithium salt. Thermal and mechanical stability of the composite polymer electrolytes were also improved by introducing PGO fillers and reasonable storage modulus values were maintained even at the elevated temperatures up to 150 °C. All-solid-state battery performance was evaluated with the composite polymer electrolyte containing 0.2 wt% of PGO, resulting in superior cycle performance compared to that of the BCP due to the enhanced ionic conductivity as well as additional ion-conducting paths provided by the PGO fillers.

Introduction

Solid polymer electrolytes (SPEs) have attracted great attention in recent years in the fields of rechargeable lithium-ion battery applications to overcome a great deal of drawbacks of conventional liquid electrolytes especially related to safety issues originating from their high volatility and flammability.[1-5] SPEs can also function as both separator and liquid electrolyte, which simplifies battery assembly and make it possible to devise flexible battery devices. However, the ionic conductivities of pure polymer materials based on poly(ethylene oxide) (PEO) are much lower than those of the conventional liquid electrolytes due to the intrinsic low mobility of ion-conducting ethylene oxide units.[3] As an attempt to enhance the ionic conductivities of the PEO derivatives, several strategies have been proposed such as blending with plasticizers having low molecular weights [6-8], incorporation of ionic liquid [9-11], and addition of plastic crystal materials such as succinonitrile.[12-14] Although ionic conductivities can be remarkably enhanced by these blending methods, the mechanical stability of the SPEs decreases because the ingredients normally soften the polymer matrix. To obtain improved ionic conductivity combined with good mechanical stability, various composite polymer electrolytes containing inorganic particles such as SiO_2, TiO_2, Al_2O_3, and ZnO have been suggested.[15, 16] These inorganic particles interact with the ion-conducting polymer matrix and the lithium salt by Lewis acid-base interactions through surface functional groups such as carboxyl and hydroxyl moieties, which promote the dissociation of the lithium salt.[17-19] Moreover, mechanical stability is also reinforced by incorporating such inorganic particles.[1]

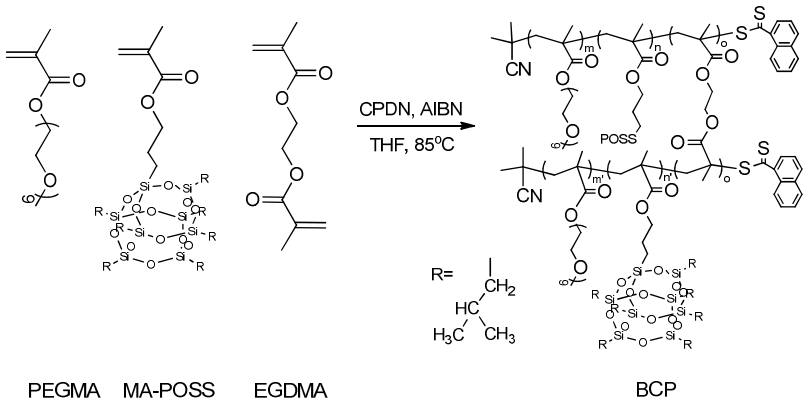

Scheme 1 Synthesis of organic/inorganic hybrid branched-graft copolymer (BCP) via RAFT polymerization.

Graphene oxide (GO) is regarded as functionalized graphene derivatives containing oxygen-bearing functional groups on its edges and basal planes.[20] GO has been utilized as filler materials of various polymer matrices for versatile applications owing to its unique chemical and physical properties.[21-24] Since GO contains various oxygen functional groups, it can increase ionic conductivity because the dissociation of the lithium salt can be increased by the interactions between the functional groups of GO and lithium ions.[25] Moreover, it has been reported that the lithium ions can potentially find low-energy conducting paths along the interface of carbon-based filler and polymer matrix.[26, 27] In addition to the high ionic conductivity, the mechanical stability of SPEs can be increased by the incorporation of GO into the polymer matrix due to the excellent mechanical strength of GO.[28] Although reduced GO has been known to be electrically conducting materials, GO and functionalized GOs exhibit insulating properties because sp^2 bonding networks are disrupted by the functionalization.[29-32] This insulating property ensures the possible application of the functionalized GOs as filler materials for the polymer electrolytes. With this respect, GO-doped ion gel as gel polymer electrolyte for all-solid-state supercapacitor was reported.[33] Still, SPEs containing GO as filler materials exhibiting pure solid-state for lithium-ion battery applications have not been reported yet.

In this study, a series of composite polymer electrolytes comprising organic/inorganic hybrid branched-graft copolymer (BCP) based on poly(ethylene glycol) methyl ether methacrylate (PEGMA) and 3-(3,5,7,9,11,13,15-heptaisobutylpentacyclo-[9.5.1.13,9.15,15.17,13]octasiloxane-1-yl)propyl methacrylate (MA-POSS) as polymer matrix and poly(ethylene glycol)-grafted graphene oxide (PGO) as filler materials were prepared and applied to the SPEs for all-solid-state lithium-ion batteries. PGO was found to be the key component to increase the ionic conductivity as well as thermal/mechanical stability of the BCP. To the best of our knowledge, it is the first time to prepare composite polymer electrolytes containing functionalized GO for the SPEs in all-solid-state lithium-ion battery applications.

Experimental

Materials

2,2'-Azobis(isobutyronitrile) (AIBN, Junsei) was recrystallized from ethanol prior to use. Poly(ethylene glycol) methyl ether methacrylate (PEGMA, average M_n = 475 g mol^{-1}) and ethylene glycol dimethylacrylate (EGDMA) was purchased from Aldrich and passed through an alumina column prior to polymerization. MethacrylisobutylPOSS® (3-(3,5,7,9,11,13,15-heptaisobutyl-pentacyclo[9.5.1.1^{3,9}.1^{5,15}.1^{7,13}]octasiloxane-1-yl)propyl methacrylate, MA-POSS) was purchased from Hybrid Plastics (product no. MA0702) and used as received. Tetrahydrofuran (THF) was freshly distilled from sodium/benzophenone under a nitrogen atmosphere. Lithium perchlorate ($LiClO_4$, >98%, Aldrich) was dried under high vacuum at 130 °C for 24 h and subsequently placed in an argon filled glove box. Graphite flakes, potassium persulfate ($K_2S_2O_8$), phosphorous pentoxide (P_2O_5), sodium nitrate ($NaNO_3$), potassium permanganate ($KMnO_4$), thionyl chloride ($SOCl_2$), poly(ethylene glycol) (PEG) (M_w = 1,000 g mol^{-1}), vanadium pentoxide (V_2O_5, 99.99 %), and *N*-Methyl-2-pyrrolidone (NMP) were purchased from Aldrich. The chain transfer agent (CTA), 2-cyanopro-2-yl-1-dithionaphthalate (CPDN) was synthesized as previously described.[34, 35] All other reagents and solvents were obtained from reliable commercial sources and used as received.

Synthesis of branched-graft poly(poly(ethylene glycol) methyl ether methacrylate-*r*-methacrylisobutyl-POSS) (BCP)

Branched poly(poly(ethylene glycol) methyl ether methacrylate-r-methacrylisobutyl-POSS) named as BCP was prepared using the RAFT polymerization.[36] PEGMA (8.64 g, 18.2 mmol), MA-POSS (5.13 g, 5.4 mmol), EGDMA (0.094 g, 0.047 mmol), CPDN (0.064 g, 0.24 mmol), and AIBN (0.012 g, 0.071 mmol) were mixed with 22 mL of distilled THF and mixture was poured into a 100 mL Schlenk flask equipped with a condenser and a magnetic stirring bar. The mixture was deoxygenated by three repeated cycles of freeze-pump-thaw method using N_2 gas, and then the RAFT polymerization was conducted at 85 °C for 21 h. After the polymerization, the solution was exposed to air and more THF was added to quench the reaction. The resulting solution was precipitated into large amount of n-hexane to remove unreacted monomers. The dissolution-precipitation cycle was repeated for three times and final polymer product was dried under vacuum at room temperature for 3 days. Finally, pink rubbery solid product was obtained with 61 % of yield. The resultant polymer was found to have 21 mol% of MA-POSS and 79 mol% of PEGMA from the ^{1}H NMR spectrum result.[36]

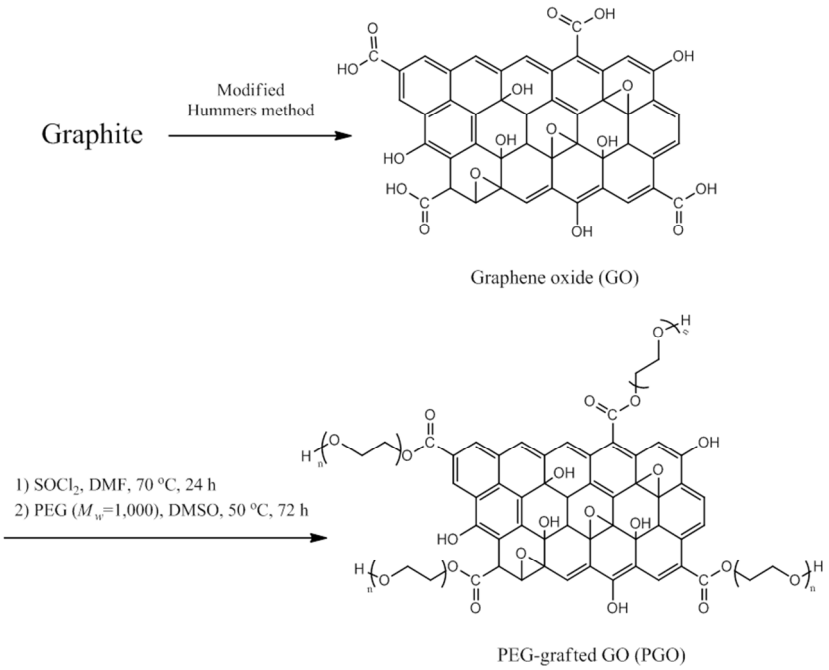

Scheme 2 Preparation of GO and PGO.

Preparation of graphene oxide (GO)

GO was prepared by the following process known as modified Hummers method.[37, 38] Preoxidation of graphite was carried out prior to the oxidation steps. Graphite flakes (1.0 g) were stirred at 80 °C for 6 h in aqueous solution of $K_2S_2O_8$ (0.5 g) and P_2O_5 (0.5 g) in concentrated H_2SO_4, followed by several washing and filtration steps with distilled water using glass frit filter equipped with anodic aluminum oxide (AAO) membrane (0.2 μm of pore size, Whatman, Germany). After dried under vacuum condition at room temperature for 24 h, the preoxidated graphite flakes were vigorously stirred at 0 °C for 40 min in a solution of $NaNO_3$ (0.5 g) in H_2SO_4. The flask was warmed up to 20 °C and $KMnO_4$ (3.0 g) was slowly added into the flask and stirred for 45 min. After that, the temperature was increased to 35 °C and the mixture was stirred for another 2 h. Brownish mixture was obtained after the temperature was raised up to 98 °C and 2.5 mL of H_2O_2 (30 wt% aqueous solution) was subsequently added into the flask to complete the oxidation steps, followed by several washing and filtration steps with 250 mL of HCl (10 wt% aqueous solution) using glass frit filter equipped with AAO membrane. To neutralize the final product, GO was thoroughly washed with the large amount of distilled water until the pH value was near 7.0 and then further dried under vacuum condition at room temperature for 48 h. Finally, 0.7 g of GO was successfully obtained with 70 % of yield.

Preparation of poly(ethylene glycol)-grafted GO (PGO)

50 mg of GO was dispersed in 20 mL of DMF under sonication for 30 min and the resultant solution was poured into 50 mL round-bottomed flask with 2-necks equipped with a magnetic stirring bar and a condenser. After the flask was charged with nitrogen gas, 10 mL of $SOCl_2$ was added by dropwise and the reaction was performed in an oil bath thermostated at 70 °C for 24 h under nitrogen atmosphere. The excess $SOCl_2$ and other byproducts were washed with distilled THF by centrifugal process for 30 min at 3000 rpm with five times. After dried under vacuum at room temperature for 1 day, the modified GO and 1.2 g of poly (ethylene glycol) (PEG) with M_w = 1,000 g mol^{-1} were dispersed in 10 mL of DMSO and the resultant solution was added to a flask equipped with a magnetic stirring bar. After the flask was charged with nitrogen gas, the reaction was performed at 50 °C for 72 h. The excess PEG was removed using ethanol by centrifugal processes with five times and the final product was dried under vacuum at room temperature for 48 h.

Preparation of composite polymer electrolytes

The solid polymer electrolytes containing BCP, $LiClO_4$, and GO (or PGO) in various compositions were prepared by a solution casting technique. For the convenience, composite polymer electrolytes containing BCP as polymer matrix and GO and PGO as filler materials are referred to as BCP-GO and BCP-PGO, respectively. Doping levels of $LiClO_4$ are defined as the ratio of the number of lithium cations (Li^+) to that of ethylene oxide (EO) repeating unit ([Li]/[EO] = 0.07) in the polymers. 0.1 g of polymers and the given amounts of $LiClO_4$ were dissolved in 0.5 mL of distilled THF and the homogeneous solutions were obtained. Various amounts of GO (or PGO) was added to the solutions and stirred at room temperature for 1 day and then additionally dispersed under sonication for 30 min right before the casting process. After that, the solution was cast onto a Teflon plate and dried at room temperature for 24 h. Subsequently, it was further dried under high vacuum at room temperature. Finally, the film was peeled off from the Teflon plate and the resultant film was placed in a high vacuum condition for a week at 60 °C prior to measure the ionic conductivities to remove residual solvent. The thickness of the films measured by a micrometer (Mitutoyo, 293-330 IP 65 water resistant) was in the range of 200-220 μm.

Cell fabrication and electrochemical characterization

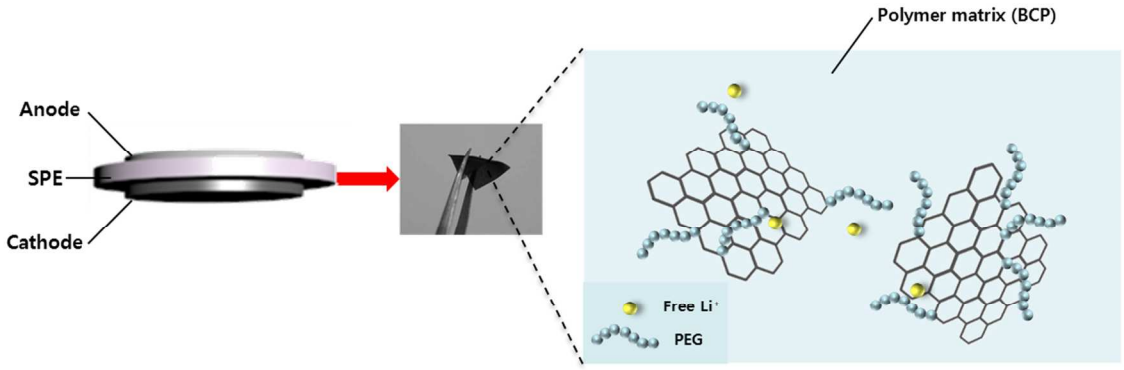

Scheme 3 Schematic illustration of composite polymer electrolyte containing PGO filler.

The ionic (t_{ion}) / electronic (t_{ele}) transport numbers and electronic conductivities of composite polymer electrolytes were determined using DC (direct-current) polarization method. A constant voltage of 50 mV was applied across the electrolyte sandwiched between two blocking stainless-steel electrodes, and polarization current as function of time was monitored for 4 hours at 30 ^{o}C under N_2 atmosphere.The electrochemical stability of composite polymer electrolytes was evaluated using linear sweep voltammetry (LSV). The cell was assembled by sandwiching electrolyte between stainless steel (working electrode) and lithium metal (reference electrode) in 2032 coin cell. The cell was swept in the potential range from 3 V to 7 V (versus Li/Li^+) at scan rate of 1 mV/s at 60 ^{o}C. Charge/discharge test of all-solid-state lithium-ion battery was performed at cutoff voltages of 2.0 ~ 3.8 V versus Li/Li^+ at 60 ^{o}C with current density of 0.1 C, where 1.0 C rate corresponds to a current density of 294 mAh. V_2O_5 (70 wt%) was used as cathode active material and dispersed in *N*-methyl-2-pyrrolidone (NMP) with carbon black (20 wt%) and PVDF (10 wt%). The resultant slurry was deposited and cast onto Aluminium current collector using doctor blade. The residual NMP was completely dried under vacuum condition at 120 ^{o}C for 1 day. The obtained cathode sheet, lithium metal, and composite polymer electrolyte were punched into disk and assembled together in 2032 coin cell to form Li/electrolyte/V_2O_5 cell. All components were prepared in argon filled glove box (H_2O < 0.5 ppm, O_2 < 0.5 ppm).

Characterization

^{1}H NMR spectra were recorded on an Ascend^{TM} 400 spectrometer (300 MHz for ^{1}H NMR) using $CDCl_3$ (Cambridge Isotope Laboratories) as the solvent at room temperature, with TMS as a reference. Solid-state ^{13}C magic angle spinning (MAS) NMR spectra were recorded on a JeolJNM-LA400 spectrometer (400 MHz) with 7 kHz MAS. Molecular weights (M_n, M_w) and polydispersity index (PDI) were analyzed by gel permeation chromatography (GPC). Relative molecular weight was measured by GPC equipped with a Waters 515 HPLC pump and three columns including PLgel 5.0 μm guard, MIXED-C and MIXED-D from Polymer Laboratories in series with a Viscotek LR125 laser refractometer. The system with a refractive index (RI) detector was calibrated using polystyrene standards from Polymer Laboratories. The resulting data was analyzed using the Omnisec software. Absolute molecular weights of polymers were analyzed using a Waters 515 HPLC pump equipped with three columns including PLgel PLgel 5.0 μm guard, MIXED-C and MIXED-D from Polymer Laboratories in series with a Wyatt Technology MiniDAWN^{TM} triple-angle light scattering detector and a Wyatt Technology Optilab DSP interferomeric refractometer. HPLC grade THF (J. T. Baker) was used as the eluent at a flow rate of 1.0 mL min^{-1} at 35 ^{o}C. The thermal transition temperatures of the polymers were examined by differential scanning calorimetry (DSC) using TA Instruments DSC-Q1000 under a nitrogen atmosphere. Samples with a typical mass of 3-7 mg were encapsulated in sealed aluminum pans. The samples were first heated to 150 ^{o}C and then quenched to -80 ^{o}C. This was followed by a second heating scan from -80 ^{o}C to 150 ^{o}C at a heating rate of 10 ^{o}C min^{-1}. The thermal stability of the polymers was investigated by thermogravimetric analysis (TGA) using TA Instruments TGA Q-5000IR under nitrogen atmosphere. The samples were maintained at 130 ^{o}C for 10 min to remove residual water molecules, and then heated to 700 ^{o}C at a heating rate of 10 ^{o}C min^{-1}. FT-IR spectra were recorded in the absorption mode on Nicolet 6700 spectrophotometer with a resolution of 4 cm^{-1} in the vibrational frequency range from 400 to 4000 cm^{-1}. X-ray photoelectron spectroscopy (XPS) measurements were performed on Axis-HIS XPS (Kratos Analyticlal, UK) using Mg Kα (1254.0 eV) as the radiation source. Field-emission scanning electron microscopy (FE-SEM) was performed on a JEOL JSM-6700F with an accelerating voltage of 10 kV. Transmission electron microscopy (TEM) was performed on a LIBRA 120 with an accelerating voltage of 120 kV. TEM specimens were prepared by drop casting of 1 wt % polymer solutions in THF on carbon-coated copper grid. Temperature-resolved rheological measurement was carried out using a rheometer (Advanced Rheometric Expansion System, ARES) in the linear viscoelastic region with 0.1 rad s^{-1} of frequency at 1 ^{o}C min^{-1} ramp. The ionic conductivity of the SPEs was analyzed by complex impedance spectroscopy between 10 to 80 ^{o}C with a Zahner Electrik IM6 apparatus in the frequency range of 0.1 Hz to 1 MHz and an applied voltage of 10 mV. The real part of the impedance at the minimum of imaginary part was used as the resistance to calculate the conductivity of the SPEs. The samples for the measurements were prepared by sandwiching the SPEs between two stainless-steel electrodes into a thickness of 200-300 μm. Each sample was allowed to equilibrate for 30 min at each temperature prior to taking measurements. The ionic conductivity (σ) was calculated from the electrolyte resistance (R) obtained from the impedance spectrum, the electrolyte thickness (d) and the area of the electrode (A) using the equation, $\sigma = (1/R) \times (d/A)$. Electrochemical stability was evaluated by linear sweep voltammetry (LSV) using a potentiostat (VMP3, Biologics) at 60 ^{o}C at scan rate of 1 mV/s. Charge/discharge test of all-solid-

state lithium-ion battery was performed with a WBCS3000 battery cycler (WonATech) at 60 °C. Electrical sheet resistivity was measured using Hiresta-UP resistivity meter (MCP-HT450). The time of electrification was 60 s and the applied voltage was 500 V. The resistivity values of GO and PGO were found to be larger than ~10^8 ohm/sq, indicating that they are insulating materials (Table S1 in the Supporting Information).

Result and discussion

Preparation of composite polymer electrolytes

A series of composite polymer electrolytes were prepared using organic/inorganic hybrid branched-graft copolymers (BCP) with poly(ethylene glycol)-grafted GO (PGO) as filler materials to study the possible applications of these materials as the SPEs in lithium-ion battery applications. A schematic illustration depicting the composite polymer electrolyte containing PGO filler is represented in Scheme 3. Recently, we reported that BCPs could be used as SPE materials for high-temperature lithium-ion batteries, although their cell performance was not sufficient for the practical applications, mostly due to the relatively low ionic conductivity of 10^{-5} S/cm at room temperature.[36] In this study, GO and/or PGO were incorporated into the BCP as filler materials to enhance the ionic conductivity and thermal/mechanical stability of the BCP. We used BCP having 21 mol % of MA-POSS and 79 mol % of PEGMA, because the BCP having this composition exhibited the highest ionic conductivity among the BCPs in solid-state at room temperature. The detailed synthetic procedure was reported previously and the structures and preparation of the BCP comprising PEGMA and MA-POSS monomeric units are represented in Scheme 1.

Synthetic procedures for the preparation of PGO from graphite are presented in Scheme 2. GO was prepared from graphite by modified Hummers method[37, 38] followed by esterification reaction between the acyl chloride group of GO activated by thionyl chloride ($SOCl_2$) and hydroxyl group of poly(ethylene glycol) (PEG, M_w = 1,000). Through this surface modification of GO, aggregation between the GO sheets decreases as well as compatibility with polymer matrix could be improved, leading to well-dispersed composite polymer electrolytes. Furthermore, PEG chains with low molecular weight grafted onto GO can increase the ionic conductivity, because the PEG chains provide additional pathway for lithium-ion conduction in the composite polymer electrolytes.

The morphology of GO and PGO fillers were investigated by TEM micrographs as shown in Fig. 1. Both micrographs of GO and PGO sheets (Fig. 1(b) and (c)) were found to be different from that of the pristine graphite (Fig. 1(a)); graphite sheets were exfoliated after the surface modification with GO and

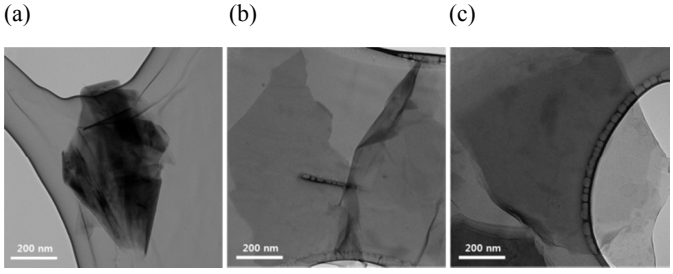

Fig. 1 TEM micrographs of (a) graphite, (b) GO, and (c) PGO.

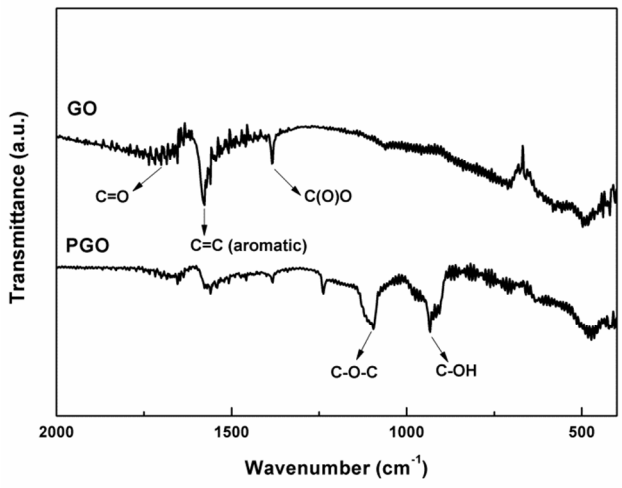

Fig. 2 FT-IR spectra of GO and PGO.

PGO, while aggregated graphite sheets were observed with the pristine graphite. The incorporation of PEG on the GO was further confirmed by IR spectroscopy as shown in Fig. 2. The absorption bands at 1350 and 1728 cm^{-1} are ascribed to the carboxylate and carbonyl groups of GO, respectively. After the PEG grafting onto the GO, a significant characteristic band corresponding to stretching vibration of C-O-C moieties of PEG is appeared at 1117 cm^{-1}, indicating that the PEG was successfully grafted onto the GO. ^{1}H NMR spectrum of PGO in the Supporting Information (Fig. S1) shows the proton signal at 3.5 ppm corresponding to ethylene oxide units of PEG, indicating that PEG chains are attached onto the GO. Although this signal is shown as a small shoulder of H_2O peak (at 3.34 ppm) due to the low intensity, the presence of the ethylene oxide units is quite obvious because such signal was not observed from ^{1}H NMR spectrum of the GO. The intensities of the carbon signals from C–OH (72 ppm) and C–O–C (60 ppm) moieties in the solid-state ^{13}C MAS NMR spectrum of PGO (Fig. S2) were found to be larger than those in GO. The XPS C 1s core-level spectra of GO and PGO in Fig. S3 show the increase in the intensity of C–O peak, and C/O ratio of PGO was 2.2 after the PEG chains were grafted onto the GO.

Incorporation of the PEG chains onto the GO was also confirmed by dispersion test of the PGO. The photographs of dispersion behavior test of PGO in various kinds of solvent with different polarity are presented in Fig. S4 in the Supporting Information. It was found out that the PGO is well-dispersed in common polar/nonpolar organic solvents, except in hexane and toluene. This excellent dispersion behavior is

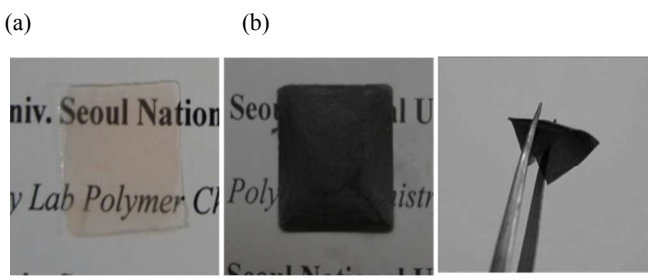

Fig. 3 Photographs of (a) pristine BCP and (b) composite polymer electrolytes having 3.0 wt% of PGO containing $LiClO_4$ ([Li]/[EO] = 0.07).

attributed to the amphiphilicity of PGO having both hydrophilic PEG groups and the relatively hydrophobic GO.[39]
Composite polymer electrolyte films containing $LiClO_4$ were prepared by mixing BCP with different amounts of GO and PGO (0.2, 0.5, 1.0, and 3.0 wt%) from solution casting method using THF as a solvent. Composite polymer electrolytes having PGO content larger than 3.0 wt% were not included, because their ionic conductivities were continuously decreased when the filler content was larger than 3.0 wt%. The lithium salt concentration was optimized as [Li]/[EO] = 0.07, which exhibited maximum ionic conductivity as shown in Fig. S5 in the Supporting Information. Dimensionally-stable free-standing films having sufficient flexibility could be obtained from all the polymer mixture as shown in Fig. 3 and Fig. S6. In the solution casting process, PGO showed much better dispersity than GO because the PEG chains grafted to GO increase the compatibility with the polymer matrix and the casting solvent. In fact, the PGO filler was well-dispersed in the polymer solution under sonication within just a few seconds, whereas the GO filler took a much longer time to be well-dispersed and required additional vigorous stirring for overnight.

Effects of PGO filler on ionic conductivity of composite polymer electrolytes

Fig. 4 shows the ionic conductivities of composite polymer electrolytes prepared by mixing BCP with GO and PGO measured at 30 °C, respectively. It was revealed that the ionic conductivities of BCP-PGO were always higher than those of the BCP-GO when the content of GO and PGO was changed from 0 to 10 wt%. The ionic conductivities of both BCP-GO and BCP-PGO increased until the filler content reached a certain amount (0.2 wt% for BCP-PGO and 0.5 wt% for BCP-GO) and start to decrease as the filler content further increases. When GO and PGO contents were smaller than 0.2 wt%, the ionic conductivities were found to be close to that of the pristine BCP (inset image in Fig. 4). When the filler contents were larger than 6.0 wt%, the ionic conductivities were found to be even smaller than that of the pristine BCP.
To further study the ionic conductivity behavior, fractions of dissociated free ions were calculated using FT-IR analysis. Fig. S7 shows the FT-IR spectra of each composite polymer electrolyte containing various contents of GO and PGO. The IR

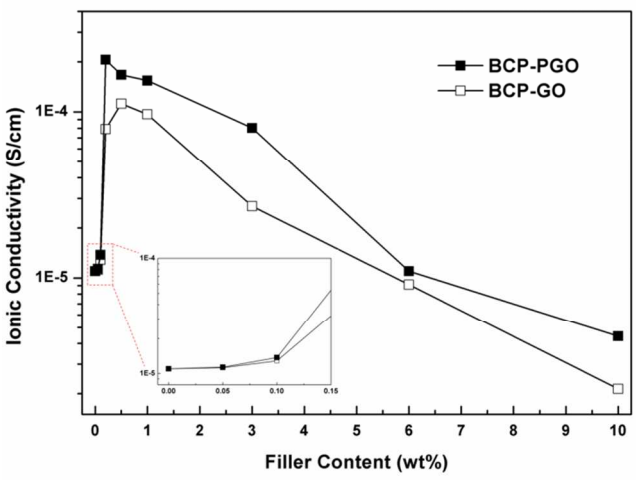

Fig. 4 Ionic conductivities of BCP-PGO and BCP-GO containing $LiClO_4$ ([Li]/[EO] = 0.07) with various filler content at 30 °C.

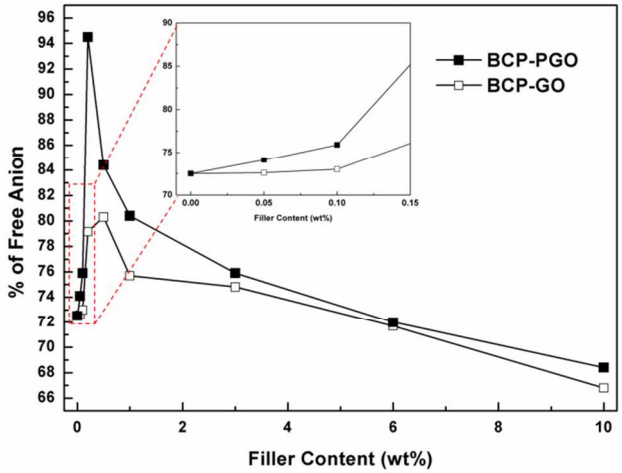

Fig. 5 Fractions of free ClO_4^- anion of BCP-GO and BCP-PGO with various filler content.

bands at 623 cm^{-1} and 635 cm^{-1} correspond to the free ClO_4^- ion and $Li^+ClO_4^-$ ion pair, respectively. To calculate the fraction of free ClO_4^- ion, the IR band in the region from 600 to 650 cm^{-1} was deconvoluted into two separated peaks (623 cm^{-1} and 635 cm^{-1}) and the area under each curve was integrated, respectively. The resulting fraction values with respect to various filler content are presented in Fig. 5. Interestingly, the changes of free ion fraction with the filler content are almost consistent with that of the ionic conductivity, indicating that the dissociation of the lithium salt significantly affects the ionic conductivity. The ionic conductivity enhances as the fraction of free ion increases, because the ionic conductivity is proportional to the number of charge carriers. Furthermore, the fractions of free ions of BCP-PGO are always larger than that of the BCP-GO, demonstrating that the grafting of PEG chains onto the GO is one of the most crucial factors in enhancing the ionic conductivity. The PEG chains grafted to the GO surface could solvate the lithium ion due to the presence of the ethylene oxide units, thereby increasing the amount of dissociated free ions. Besides the PEG chains, COOH and OH groups of the GO can also interact with the lithium salt by Lewis acid-base interactions, thereby further promoting the dissociation of the lithium salt into free ions.[40] Thus, the free ion contents in BCP-GO are always larger than that in the BCP, the pristine polymer matrix.
Another reason for the higher ionic conductivities of BCP-PGO than those of BCP-GO is ascribed to good dispersion state of

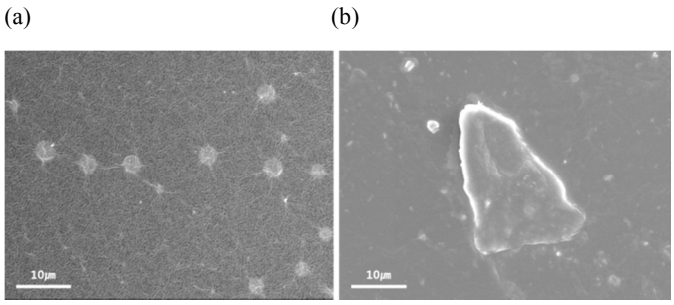

Fig. 6 SEM images of (a) BCP-PGO and (b) BCP-GO composite polymer electrolyte (filler content = 3 wt%)

PGO in the polymer matrix. In order to evaluate the effect of PEG grafting on the dispersion behavior of the fillers, SEM images of composite polymer electrolytes containing same amount (3.0 wt%) of GO and PGO were taken, respectively, as shown in Fig. 6; PGO fillers are more or less well-dispersed in the entire polymer matrix (Fig. 6(a)), whereas serious aggregation was observed for the GO fillers (Fig. 6(b)). Cross-sectional SEM images of BCP-GO and BCP-PGO are also presented in Fig. S8 in the Supporting Information. The better dispersion of the PGO in polymer matrix is mainly due to the increased compatibility of the PEG chains on the GO.[41] It is desirable for the fillers to be well-dispersed in the polymer matrix to provide increased effective interfacial area between the filler and lithium salt, which can increase the dissociation of the lithium salt, while large clusters of filler can even serve as a barrier that can disturb ion transport.[42] Furthermore, the homogeneous distribution of PGO fillers in the polymer matrix provides additional ion-conducting paths that facilitate lithium-ion transport, resulting in higher conductivity compared to that of the pristine BCP.[33] This dispersion behavior might additionally explain why BCP-PGO needed a smaller amount (0.2 wt%) of the filler, PGO, to exhibit the maximum ionic conductivity and fraction of free ions than BCP-GO (0.5 wt%).

The glass transition temperature (T_g) is another important factor affecting ionic conductivities. As shown in Fig. 7, the T_g of the P(PEGMA) segment in BCP continuously increases with filler content, because the rigid characteristic of both GO and PGO decreases the chain mobility of ion-conducting P(PEGMA) segments.[43-45] DSC thermograms of BCP-PGO and BCP-GO are presented in Fig. S9 in the Supporting Information. For example, the addition of only 1.0 wt% of GO and PGO increases the T_g by more than 20 °C. However, even if the chain mobility of the ion-conducting segments decreases, the ionic conductivities of composite polymer electrolytes are always higher than those of the pristine BCP, because they have larger amount of dissociated free ions and additional ion-conducting paths as described previously. However, when the filler content is larger than 0.5 wt%, the ionic conductivities of both BCP-GO and BCP-PGO decreases continuously, because the positive effect of the fillers is offset by further decrease in the chain mobility of ion-conducting segments. Furthermore, it was found that the T_gs of P(PEGMA) segments of BCP-PGO are lower than those of the BCP-GO throughout the entire filler content. This could be attributed to plasticization effect of the grafted PEG chains on the PGO. Similar behavior was reported for polymer-functionalized CNT composites.[46]

As a result, the maximum ionic conductivity of 2.1×10^{-4} S/cm at 30 °C was obtained when 0.2 wt% of PGO was incorporated, and this value is about one order of magnitude higher than that of the pristine BCP (1.1×10^{-5} S/cm at 30 °C) and comparable or even slightly higher than those of other reported SPEs in pure solid states at room temperature.

Thermal and mechanical properties

In addition to the high ionic conductivity, thermal and mechanical stability is another important characteristic of the SPEs to use them for high-performance lithium-ion batteries.[47, 48] To evaluate the thermal stability of the fillers, thermogravimetric analysis (TGA) was conducted and the TGA curves of graphite, GO, and PGO are presented in Fig. 8. GO has been known to show an abrupt weight loss with an onset temperature at around 200 °C, corresponding to the decomposition of the oxygen functional groups attached on the GO surfaces.[41, 49] Such an abrupt weight change at about 200 °C was not observed with PGO, indicating that the PEG chains attached on the oxygen functional groups on the GO increase the thermal stability. The inter- and intra- molecular interaction between the filler and the polymer chains attached on GO has been known to increase the thermal stability of GO.[41] For example, when vinyl polymers such as polystyrene, poly(methyl methacrylate), and poly(2-(dimethylamino)ethyl methacrylate) were introduced on the GO, similar increase of the thermal stability were observed.[50-52]

Furthermore, when PGO was incorporated in the BCP, the thermal stability of BCP was found to increase as shown in the Supporting Information (Fig. S10). For example, when the PGO content in BCP-PGO is 3.0 wt%, the temperature for 25 % weight loss increases by almost 40 °C, from 295 °C to 334 °C. This could be also attributed to the enhanced interaction between polymer matrix and PGO, resulting in slower decomposition phenomenon.[53] Moreover, the PGO having oxygen functional groups including hydroxyl groups can serve as both radical scavenger and barrier against oxygen and degraded product, thereby delaying the permeation of oxygen into the composite and escape of volatile degraded products.[41, 54]

To figure out the effects of PGO filler content on the mechanical stability of the composite polymer electrolytes,

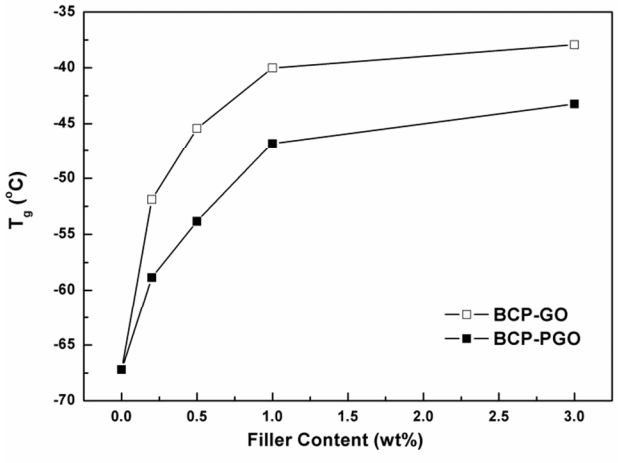

Fig. 7 Glass transition temperatures of P(PEGMA) segments in BCP with various filler content.

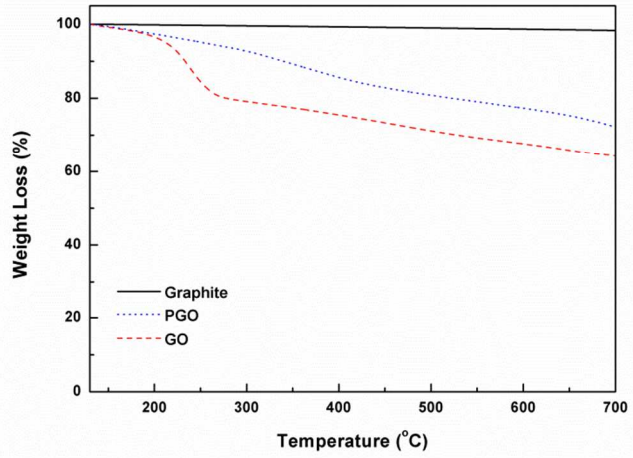

Fig. 8 TGA profiles of graphite, PGO, and GO with a heating rate of 10 °C min^{-1}.

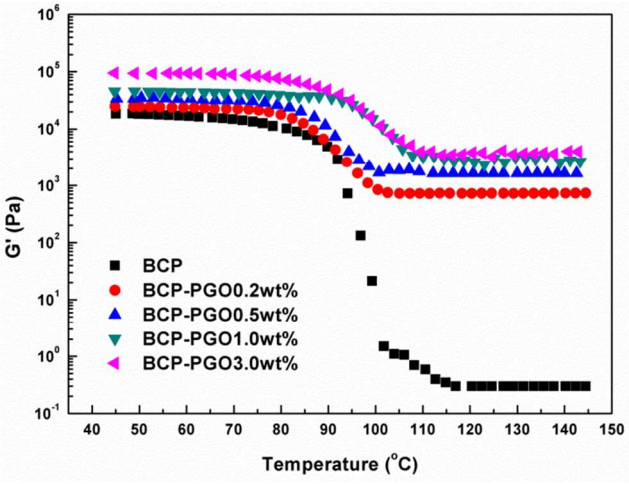

Fig. 9 Temperature-resolved rheological behaviors of BCP-PGO containing different PGO content in the linear viscoelastic region with 0.1 rad s^{-1} of frequency at 1 °C min^{-1} ramp.

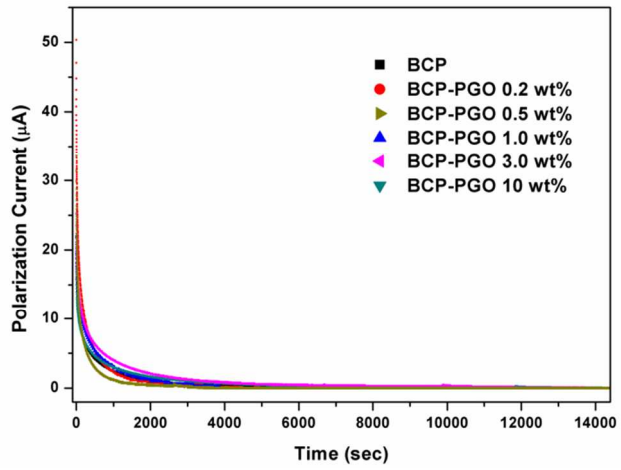

Fig. 10 Polarization current curves of BCP and BCP-PGOs containing various PGO contents.

temperature-resolved rheological behaviors of each electrolyte having different contents of PGO filler were measured (Fig. 9). BCP and BCP-PGOs show almost constant storage modulus (G') values until the temperature reaches to 80 °C, indicating that the solid film property could be maintained until 80 °C. The G' values of the samples decrease when the temperature increases further, while the decrease is much less for the BCP-PGOs. The decrease of G' values from 80 °C could be ascribed to the glass transition temperature of the BCP (Fig. S11). It is noteworthy that the G' values of BCP-PGOs are much larger than that of the BCP for the entire temperature range and the BCP-PGOs having larger contents of PGO have larger G' values. Furthermore, only 0.2 wt% of PGO addition into BCP increases the G' value by more than 4 orders of magnitude at elevated temperatures (> 100 °C). For example, the G' values of BCP-PGO (0.2 wt%) and BCP are 3.8×10^3 Pa and 3.0×10^{-1} Pa at 120 °C, respectively.

Evaluation of ionic/electronic transport

Electrolytes of lithium-ion batteries should be electronic insulator to exclude operational problems such as formation of short-circuit and self-discharge. To ensure the insulating properties of composite polymer electrolytes containing PGO fillers, ionic/electronic transport numbers and electronic conductivities were evaluated from DC polarization method.[59, 60] A constant voltage of 50 mV was applied to the symmetric cell having configuration of SS/polymer electrolyte/SS, where SS indicates stainless-steel, and then polarization current as function of time was monitored until the current value reaches steady-state (Fig. 10). The initial total current (I_t) is attributed to the combined mobility of both ionic species and electron. The current decreases with time due to the polarization of mobile ions at the electrode/electrolyte interface, and then the residual current at steady-state (I_e) is observed corresponding to the mobility of only electron. From the polarization current curves, ionic (t_{ion}) and electronic (t_{ele}) transport numbers can be determined using following equations (1) and (2):

$$t_{ion} = I_t - I_e / I_t \quad (1)$$

$$t_{ele} = I_e / I_t \quad (2)$$

where $t_{ion} + t_{ele} = 1$. The resultant transport numbers and electronic conductivities of composite polymer electrolytes are presented in Table S2 in the Supporting Information. Both electronic transport numbers and electronic conductivities of each composite polymer electrolyte can be negligible, indicating that the BCP-PGOs have insulating properties enough to exclude the operational problems.[60, 61]

Electrochemical performance of all-solid-state lithium-ion battery

The electrochemical stabilities of pristine BCP, BCP-GO, and BCP-PGO were evaluated using linear sweep voltammetry with a SS (Stainless steel)/SPE/Li coin cell at 60 °C. Fig. 11 shows the linear sweep voltammogram of the BCP and BCP having the largest amount of GO and PGO (3.0 wt%). The abrupt rise in current at the certain voltage corresponds to the electrochemical oxidative degradation of the electrolyte, and the decomposition voltages of pristine BCP, BCP-GO, and BCP-PGO were found to be close at about 5.3 V (vs. Li/Li^+). Other composite polymer electrolytes containing smaller contents of the fillers also exhibited similar electrochemical

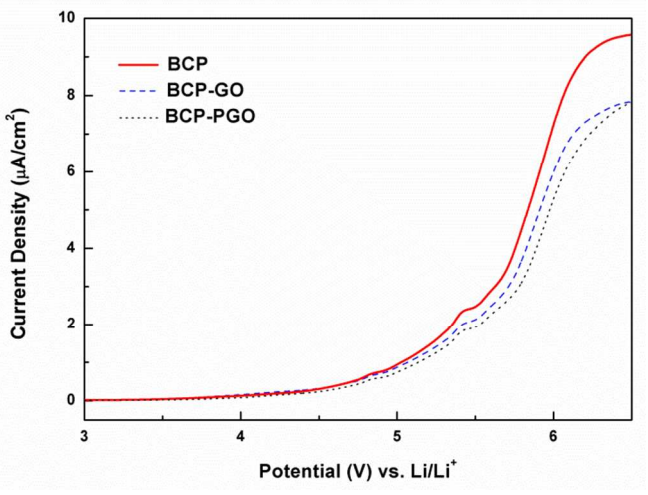

Fig. 11 Linear sweep voltammogram of BCP, BCP-GO (3.0 wt%), and BCP-PGO (3.0 wt%) at 60 °C with scan rate of 1 mV/s.

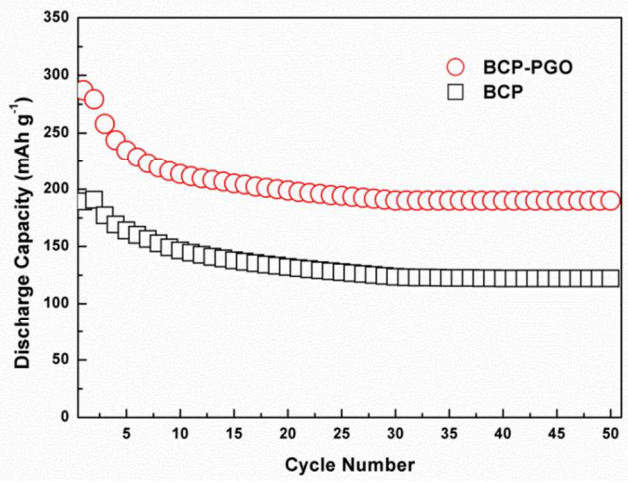

Fig. 12 Discharge capacity profiles of all-solid-state Li/SPE/V_2O_5 cell (SPE: pristine BCP and BCP-PGO (0.2 wt%)) cycled at 60 °C with scan rate of 0.1 C.

stability. Therefore, it can be concluded that all the composite polymer electrolytes are electrochemically stable within the operation voltage range of V_2O_5 cathode, as well as other 4 V class cathode materials.

Cyclic performances of all-solid-state Li/SPE/V_2O_5 cells with pristine BCP and BCP-PGO having 0.2 wt% of PGO were tested at 60 °C cycled at 0.1 C rate, respectively (Fig. 12). The cyclic performances were evaluated at 60 °C, because the advantage of the all-solid-state batteries is that they could be operated at elevated temperature without causing safety problem. Also, since the ionic conductivity of pristine BCP at room temperature is quite low as 10^{-5} S/cm, it was not possible to test the cyclic performance of the cell prepared using the BCP only. Therefore, the comparison of the cell performances between the pristine BCP and BCP-PGO was not possible at room temperature. The charge/discharge curves of each cell are presented in Fig. S12 in the Supporting Information. BCP-PGO having 0.2 wt% of PGO was chosen for the cell test because it exhibited the highest ionic conductivity among the composite polymer electrolytes. Compared to the pristine BCP, relatively higher initial discharge capacity of 287 mAh g^{-1} was observed from BCP-PGO, which is close to the theoretical capacity of V_2O_5 cathode (294 mAh g^{-1} for intercalation of two Li^+). This result is ascribed to the higher ionic conductivity of the BCP-PGO electrolyte than that of the pristine BCP, which contributes to the fast lithium-ion transport. The facile ionic transport alleviates the ohmic polarization loss of the cell, leading to the larger capacity.[8, 55] It is worthy to note that only 0.2 wt% of PGO can effectively improves cyclic performance of the all-solid-state lithium-ion battery. Still, about 30 % of initial capacity loss during first 10 cycles was observed although no further significant decrease was observed. Similar initial decreases in capacity have been reported in all-solid-state lithium-ion battery system.[56, 57] The capacity loss in the solid system was likely due to an increase of charge transfer resistance since the interfaces between the cathode materials and SPE are relatively unstable due to the solid nature of the electrolyte. In contrast, no such decrease is observed in lithium-ion battery systems using liquid electrolytes, because the liquid electrolyte can readily soak into the electrode. It was also reported that the binding capability of the PVDF binder decreased when the temperature is higher than 60 °C leading to performance deterioration in lithium-ion batteries.[58] Therefore, further work is likely to improve the capacity retention by changing the polymeric binder materials and the compositions of the electrode components.

Conclusions

In this study, PEG-grafted graphene oxide (PGO) was synthesized to be used as filler material for the solid-state polymer electrolytes in lithium-ion battery applications. By introducing small amount of PGO, ionic conductivity, thermal/mechanical stability, and cyclic performance were dramatically improved compared to those of pristine polymer matrix. A maximum ionic conductivity of 2.1×10^{-4} S/cm at 30 °C was achieved, which is one order of magnitude higher than that of the pristine polymer matrix when only 0.2 wt% of PGO was incorporated, mainly due to an increase in the dissociation of the lithium salt by Lewis acid-base interaction between the PGO and lithium salt. The solid-state of polymer electrolytes and the relatively high storage modulus values were maintained even at the elevated temperatures (~150 °C), demonstrating the significant reinforcement effect of PGO filler. All-solid-state battery test with composite polymer electrolyte containing 0.2 wt% of optimized PGO content exhibited superior cycle performance compared to that of the pristine polymer matrix, which is attributed to the high ionic conductivity and long-term cyclic stability originating from the excellent mechanical stability of the PGO. All of the improved properties of the composite polymer electrolyte containing the PGO filler suggest that PGO is very effective and promising filler material which can be universally applied to any kinds of polymer matrix to enhance the electrochemical performance of all-solid-state lithium-ion batteries even at the elevated temperature (60 °C).

Acknowledgements

This research was supported by the Technology Innovation Program (grant number: 10045221) funded by the Ministry of Trade, Industry and Energy (MOTIE, Korea).

Notes and references

School of Chemical and Biological Engineering and Institute of Chemical Processes, Seoul National University, 599 Gwanak-ro, Gwanak-gu, Seoul 151-742, Republic of Korea. Fax: +82-02-880-8899; Tel: +82-02-880-7070; E-mail: jongchan@snu.ac.kr

Electronic Supplementary Information (ESI) available: [details of any supplementary information available should be included here]. See DOI: 10.1039/b000000x/

1 A. Manuel Stephan and K. S. Nahm, *Polymer*, 2006, **47**, 5952-5964.
2 W. H. Meyer, *Adv. Mater.*, 1998, **10**, 439-448.
3 J. M. Tarascon and M. Armand, *Nature*, 2001, **414**, 359-367.
4 S. K. Kim, D. G. Kim, A. Lee, H. S. Sohn, J. J. Wie, N. A. Nguyen, M. E. Mackay and J. C. Lee, *Macromolecules*, 2012, **45**, 9347-9356.
5 D. G. Kim, H. S. Sohn, S. K. Kim, A. Lee and J. C. Lee, *J. Polym. Sci., Part A: Polym. Chem.*, 2012, **50**, 3618-3627.
6 X. Q. Yang, H. S. Lee, L. Hanson, J. McBreen and Y. Okamoto, *J. Power Sources*, 1995, **54**, 198-204.
7 L.-Z. Fan, X.-L. Wang, F. Long and X. Wang, *Solid State Ionics*, 2008, **179**, 1772-1775.
8 D. G. Kim, J. M. Shim, J. H. Lee, S. J. Kwon, J. H. Baik and J. C. Lee, *Polymer*, 2013, **54**, 5812-5820.

9 J.-H. Shin, W. A. Henderson and S. Passerini, *Electrochem. Commun.*, 2003, **5**, 1016-1020.
10 T. Sato, T. Morinaga, S. Marukane, T. Narutomi, T. Igarashi, Y. Kawano, K. Ohno, T. Fukuda and Y. Tsujii, *Adv. Mater.*, 2011, **23**, 4868-4872.
11 J. H. Lee, J. S. Lee, J. W. Lee, S. M. Hong and C. M. Koo, *Eur. Polym. J.*, 2013, **49**, 1017-1022.
12 L. Z. Fan, X. L. Wang and F. Long, *J. Power Sources*, 2009, **189**, 775-778.
13 A. M. Christie, S. J. Lilley, E. Staunton, Y. G. Andreev and P. G. Bruce, *Nature*, 2005, **433**, 50-53.
14 A. Abouimrane, Y. Abu-Lebdeb, P. J. Alarco and M. Armand, *J. Electrochem. Soc.*, 2004, **151**, A1028-A1031.
15 F. Croce, L. Persi, F. Ronci and B. Scrosati, *Solid State Ionics*, 2000, **135**, 47-52.
16 S. H. Chung, Y. Wang, L. Persi, F. Croce, S. G. Greenbaum, B. Scrosati and E. Plichta, *J. Power Sources*, 2001, **97–98**, 644-648.
17 X. L. Hu, G. M. Hou, M. Q. Zhang, M. Z. Rong, W. H. Ruan and E. P. Giannelis, *J. Mater. Chem.*, 2012, **22**, 18961-18967.
18 A. M. Stephan and K. S. Nahm, *Polymer*, 2006, **47**, 5952-5964.
19 Z. X. Wang, X. J. Huang and L. Q. Chen, *Electrochem. Solid-State Lett.*, 2003, **6**, E40-E44.
20 D. R. Dreyer, S. Park, C. W. Bielawski and R. S. Ruoff, *Chem Soc Rev*, 2010, **39**, 228-240.
21 X. Huang, X. Y. Qi, F. Boey and H. Zhang, *Chem. Soc. Rev.*, 2012, **41**, 666-686.
22 S. Stankovich, D. A. Dikin, G. H. B. Dommett, K. M. Kohlhaas, E. J. Zimney, E. A. Stach, R. D. Piner, S. T. Nguyen and R. S. Ruoff, *Nature*, 2006, **442**, 282-286.
23 H. Kim, A. A. Abdala and C. W. Macosko, *Macromolecules*, 2010, **43**, 6515-6530.
24 J. R. Potts, D. R. Dreyer, C. W. Bielawski and R. S. Ruoff, *Polymer*, 2011, **52**, 5-25.
25 C. Tang, K. Hackenberg, Q. Fu, P. M. Ajayan and H. Ardebili, *Nano Lett.*, 2012, **12**, 1152-1156.
26 C. Y. Tang, K. Hackenberg, Q. Fu, P. M. Ajayan and H. Ardebili, *Nano Lett.*, 2012, **12**, 1152-1156.
27 A. Udomvech, T. Kerdcharoen and T. Osotchan, *Chem. Phys. Lett.*, 2005, **406**, 161-166.
28 M. A. Rafiee, J. Rafiee, Z. Wang, H. Song, Z.-Z. Yu and N. Koratkar, *ACS Nano*, 2009, **3**, 3884-3890.
29 C. Gomez-Navarro, R. T. Weitz, A. M. Bittner, M. Scolari, A. Mews, M. Burghard and K. Kern, *Nano Lett.*, 2007, **7**, 3499-3503.
30 Y. Si and E. T. Samulski, *Nano Lett.*, 2008, **8**, 1679-1682.
31 B. Xu, S. F. Yue, Z. Y. Sui, X. T. Zhang, S. S. Hou, G. P. Cao and Y. S. Yang, *Energy Environ. Sci.*, 2011, **4**, 2826-2830.
32 J. L. Zhang, G. X. Shen, W. J. Wang, X. J. Zhou and S. W. Guo, *J. Mater. Chem.*, 2010, **20**, 10824-10828.
33 X. Yang, F. Zhang, L. Zhang, T. F. Zhang, Y. Huang and Y. S. Chen, *Adv. Funct. Mater.*, 2013, **23**, 3353-3360.
34 H. S. Sohn, S. H. Cha, W. K. Lee, D. G. Kim, H. J. Yun, M. S. Kim, B. D. Kim, Y. H. Kim, J. W. Lee, J. S. Kim, D. B. Kim, J. H. Kim and J. C. Lee, *Macromol. Res.*, 2011, **19**, 722-728.
35 J. Zhu, X. L. Zhu, Z. P. Cheng, F. Liu and J. M. Lu, *Polymer*, 2002, **43**, 7037-7042.
36 J. Shim, D.-G. Kim, J. H. Lee, J. H. Baik and J.-C. Lee, *Polym. Chem.*, 2014, **5**, 3432-3442.
37 W. S. Hummers and R. E. Offeman, *J. Am. Chem. Soc.*, 1958, **80**, 1339-1339.
38 S. Stankovich, D. A. Dikin, R. D. Piner, K. A. Kohlhaas, A. Kleinhammes, Y. Jia, Y. Wu, S. T. Nguyen and R. S. Ruoff, *Carbon*, 2007, **45**, 1558-1565.
39 X. Y. Qi, K. Y. Pu, H. Li, X. Z. Zhou, S. X. Wu, Q. L. Fan, B. Liu, F. Boey, W. Huang and H. Zhang, *Angew. Chem. Int. Ed.*, 2010, **49**, 9426-9429.
40 D. Zhou, X. G. Mei and J. Y. Ouyang, *J. Phys. Chem. C*, 2011, **115**, 16688-16694.
41 S. P. Zhang, P. Xiong, X. J. Yang and X. Wang, *Nanoscale*, 2011, **3**, 2169-2174.
42 Q. Li, E. Wood and H. Ardebili, *Appl. Phys. Lett.*, 2013, **102**.
43 S. Vadukumpully, J. Paul, N. Mahanta and S. Valiyaveettil, *Carbon*, 2011, **49**, 198-205.
44 Y. H. Xue, Y. Liu, F. Lu, J. Qu, H. Chen and L. M. Dai, *J. Phys. Chem. Lett.*, 2012, **3**, 1607-1612.
45 T. Ramanathan, A. A. Abdala, S. Stankovich, D. A. Dikin, M. Herrera-Alonso, R. D. Piner, D. H. Adamson, H. C. Schniepp, X. Chen, R. S. Ruoff, S. T. Nguyen, I. A. Aksay, R. K. Prud'homme and L. C. Brinson, *Nat. Nanotechnol.*, 2008, **3**, 327-331.
46 G. L. Hwang, Y. T. Shieh and K. C. Hwang, *Adv. Funct. Mater.*, 2004, **14**, 487-491.
47 J. B. Goodenough and Y. Kim, *Chem. Mater.*, 2010, **22**, 587-603.
48 V. Etacheri, R. Marom, R. Elazari, G. Salitra and D. Aurbach, *Energy Environ. Sci.*, 2011, **4**, 3243-3262.
49 S. H. Lee, D. R. Dreyer, J. H. An, A. Velamakanni, R. D. Piner, S. Park, Y. W. Zhu, S. O. Kim, C. W. Bielawski and R. S. Ruoff, *Macromol. Rapid Commun.*, 2010, **31**, 281-288.
50 M. Fang, K. G. Wang, H. B. Lu, Y. L. Yang and S. Nutt, *J. Mater. Chem.*, 2009, **19**, 7098-7105.
51 G. Goncalves, P. A. A. P. Marques, A. Barros-Timmons, I. Bdkin, M. K. Singh, N. Emami and J. Gracio, *J. Mater. Chem.*, 2010, **20**, 9927-9934.
52 Y. F. Yang, J. Wang, J. Zhang, J. C. Liu, X. L. Yang and H. Y. Zhao, *Langmuir*, 2009, **25**, 11808-11814.
53 V. H. Pham, T. T. Dang, S. H. Hur, E. J. Kim and J. S. Chung, *Acs Appl. Mater. Inter.*, 2012, **4**, 2630-2636.
54 Y. W. Cao, Z. L. Lai, J. C. Feng and P. Y. Wu, *J. Mater. Chem.*, 2011, **21**, 9271-9278.
55 H. J. Ha, E. H. Kil, Y. H. Kwon, J. Y. Kim, C. K. Lee and S. Y. Lee, *Energy Environ. Sci.*, 2012, **5**, 6491-6499.
56 P. P. Prosini, Y. Y. Xia, T. Fujieda, R. Vellone, M. Shikano and T. Sakai, *Electrochim. Acta*, 2001, **46**, 2623-2629.
57 B. Sun, I. Y. Liao, S. Tan, T. Bowden and D. Brandell, *J Power Sources*, 2013, **238**, 435-441.
58 T. Yoon, S. Park, J. Mun, J. H. Ryu, W. Choi, Y. S. Kang, J. H. Park and S. M. Oh, *J. Power Sources*, 2012, **215**, 312-316.
59 N. Shukla and A. K. Thakur, *Solid State Ionics*, 2010, 181, 921-932.
60 S. R. Mohapatra, A. K. Thakur and R. N. P. Choudhart, *J. Power Sources*, 2009, **191**, 601-613.
61 C. A. C. Sequeira, M. J. C. Plancha and L. P. S. Araujo, *J. Phys. IV*, 1994, **4**, 17-35.

Graphical Abstract

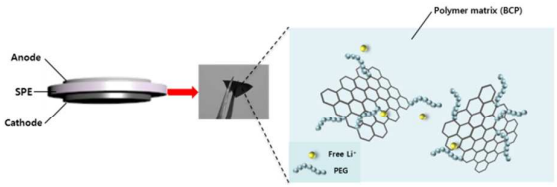

A series of composite polymer electrolytes containing poly(ethylene glycol)-grafted graphene oxide fillers were prepared for all-solid-state lithium-ion battery applications.